Single Molecule Magnetism in Linear Fe(I) Complexes with Aufbau and non-Aufbau ground-state

Rishu Khurana and Md. Ehesan Ali*

Institute of Nano Science and Technology, Sector-81, Mohali, Punjab-140306, India

E-mail: ehesan.ali@inst.ac.in

Abstract

With the ongoing efforts on synthesizing mono-nuclear single-ion magnets (SIMs) with promising applications in high-density data storage and spintronics devices, the linear Fe(I) complexes emerge as the enticing candidates possessing large unquenched angular momentum. Herein, we have studied five experimentally synthesized linear Fe(I) complexes to uncover the origin of single-molecule magnetic behavior of these complexes. To begin with, we benchmarked our methodology on the experimentally and theoretically well studied complex, $[\text{Fe}\{\text{C(SiMe}_3)\}_3]^{-1}$ **(1)** (SiMe$_3$ = trimethylsilyl) which is characterized with large spin-reversal barrier of 226 cm^{-1} [Nat. Chem. **2013**, *5*, 577–581]. Further, the two Fe(I) complexes, i.e., $[\text{Fe(cyIDep)}_2]^{+1}$ **(2)** ((cyIDep = 1,3-bis(2′,6′-diethylphenyl)-4,5-(CH$_2$)$_4$-imidazol-2-ylidene) and $[\text{Fe(sIDep)}_2]^{+1}]$ **(3)** (sIDep = 1,3-bis(2′,6′-diethylphenyl)-imidazolin-2-ylidene) are studied that do not possess SIM behavior under ac or dc magnetic fields, however, they are reported to exhibit large opposite axial zero field splitting (-62.4 and +34.0 cm^{-1} respectively) from *ab initio* calculations. Employing state-of-the-art *ab initio* calculations, we have unwrapped the origin of this contrasting observation between experiment and theory by probing

their magnetic relaxation pathways and the pattern of d-orbitals splitting. Additionally, the two experimentally synthesized Fe(I) complexes, i.e., $[(\eta^6\text{-}C_6H_6)FeAr^*\text{-}3,5\text{-}Pr^i_2]$ **(4)** $(Ar^*\text{-}3,5\text{-}Pr^i_2 = C_6H\text{-}2,6\text{-}(C_6H_2\text{-}2,4,6\text{-}Pr^i_3)_2\text{-}3,5\text{-}Pr^i_2)$ and $[(CAAC)_2Fe]^{+1}$ **(5)** $(CAAC =$ cyclic (alkyl)(amino)carbene) are investigated for SIM behavior, since there is no report on their magnetic properties. To this end, complex **4** presents itself as the potential candidate for SIM.

1 Introduction

Single-ion magnets (SIMs) are the centrepiece of numerous areas of research with promising applications in quantum computing,[1,2] molecular spintronics,[3] classical data storage[4] etc. These are distinct molecules displaying slow relaxation of magnetization that is characterized by an energy barrier (U_{eff}) for reversal of total molecular spin. The energy barrier further depends on the total spin of the system and is given by $U_{eff} = S^2|D|$ and $(S^2\text{-}1/4)|D|$ (for integer and non-integer spin states respectively), where D is the axial zero field splitting parameter.[5] Complexes based on lanthanides (Ln) have gained much popularity as propitious candidates for SIMs since the report of phthalocyanine Tb(III) complex, TbPc$_2$ in 2003 owing to huge magnetic anisotropy and large spin ground state.[6] Followed by this, a plethora of Ln-based complexes have been synthesized and characterized with high anisotropic energy barriers. They exhibit large unquenched angular momentum and strong spin-orbit coupling, which are solely responsible for their magnetic behaviors.[7–12]

Transition metal (TM) complexes have also entered the spotlight in recent years, offering tantalizing alternatives to be utilized in prospective applications.[13–15] In this regard, in mononuclear complexes containing 3d-metal ions, it is essential to maintain the first-order orbital angular momentum to accomplish large magnetic anisotropy on a level comparable with Ln based complexes.[16,17] Controlling various chemical modifications in the coordination environment, such as the coordination number, geometry of the complex and nature of ligand atoms directly bonded to the metal center, assists in the conservation of the first-order

orbital angular momentum. In TM complexes with coordination number greater than 4, the ligand field largely quenches the orbital angular momentum as a result of Jahn Teller distortion.[18] However, the complexes with high axial symmetry, show signs of unquenched angular momentum and hence moderate magnetic anisotropy, but the molecules with high local symmetry are quite scarce.[19] The breaking of symmetry significantly lowers the magnitude of magnetic anisotropy as elegantly reported by Feng et al. where the Fe(III) complex i.e. $[(PMe_3)_2FeCl_3]$ with appropriate local symmetry results in D = -50 cm^{-1} which lowers to -17 cm^{-1} in $[(PMe_2Ph)_2FeCl_3]$ complex with the broken symmetry.[20] Prompted by the high D value for the symmetrical Fe(III) TBP complex, we also modelled 14 complexes by varying the axial ligands with Group 15 elements and equatorial ligands with halides on the reported symmetrical complex $[(PMe_3)_2FeCl_3]$ and obtained significant D values in the range -40 to -60 cm^{-1} for 8 complexes.[21] To overcome these ligand field effects, the low-coordinate complexes (coordination number <4) renewed the interest of researchers, since, they favor degenerate ground states resulting in minimal quenching of orbital angular momentum. To this end, linear or quasi-linear two-coordinate complexes emerge as the choicest complexes for mitigating these effects and eventually resulting in large anisotropic energy barriers.[22–25] The stability and isolation of these low coordinated complexes necessitate sterically encumbered ligands. A copious number of two- and three-coordinate complexes featuring Fe(II) center are already reported with intriguing magnetic properties.[13,15,26–28] Nearly, all these complexes anchorage sterically bulky ligands. However, in Fe(II) based complexes, the slow relaxation of magnetization is observed only in the presence of d.c. field owing to Fe(II) being a non-Kramer ion. Therefore, taking advantage of Kramer's theorem and thus, attenuating quantum tunneling of magnetization (QTM) within ground doublet, Zadrozny et al. reported the first prominent example of two coordinate complex of Fe(I) i.e. $[Fe(C(SiMe_3)_3)_2]^-$ with an exceptionally high energy barrier of 226 cm^{-1} under zero applied field.[29,30] Later on, Werncke et al. reported another Fe(I) complex, $[Fe(N(SiMe_3)_2)_2]^-$, but with a very small energy barrier of 64 cm^{-1} which is attributed to the reduced symmetry of the complex.[31]

Another Fe(I) complex $[Fe(N(SiMe_3)Dipp)_2]^-$ (Dipp = C_6H_3-2,6-Pr^i_2) was synthesized by Power et al. and characterized with the sizable D value of -65 cm^{-1}.[32] Further, two linear and one T-shaped Fe(I) complexes employing bulky NHC (N-heterocyclic carbene) ligands were synthesized by Ouyang et al.[33] Later on, they carried the magnetic characterization of these complexes explaining multiple magnetic relaxation pathways existing in the three co-ordinate complexes.[34] Another Fe(I) complex $[Cp^{Ar}Fe(IiPr_2Me_2)]$ (Cp^{Ar} =$C_5(C_6H_4$-4-Et$)_5$; $IiPr_2Me_2$ =1,3-diiso-propyl-4,5-dimethylimidazolin-2-ylidene) has been synthesized and characterized with spin-reversal barrier of 64 cm^{-1} by Chakraborty et al.[35]

In recent years, although two-coordinate Fe(I) complexes with sterically bulky ligands have been synthesized,[33,36,37] but a thorough study to underpin the origin of magnetic anisotropy in these complexes has not been done yet. The present work aims to gain an in-depth understanding of magnetic anisotropy in a series of linear two-coordinate Fe(I) complexes, employing state-of-the-art *ab initio* calculations. To this end, we have chosen 5 experimentally reported Fe(I) complexes, namely, $[Fe\{C(SiMe_3)\}_3]^{-1}$ **(1)**,[30] $[Fe(cyIDep)_2]^{+1}$ **(2)**, $[Fe(sIDep)_2]^{+1}]$ **(3)**,[33] $[(\eta^6$-$C_6H_6)FeAr^*$-3,5-$Pr^i_2]$ **(4)**[36] and $[(CAAC)_2Fe]^{+1}$ **(5)**[37] as shown in Figure 1. Since complex **1** is experimentally characterized with high spin-reversal barrier, it is plumped for benchmarking the methodology. Complexes **2** and **3** are experimentally synthesized and are reported to possess large axial zero field splitting parameter with opposite signs (-62.4 cm^{-1} for **2** and +34.0 cm^{-1} for **3**) from *ab initio* DDCI3 calculations. Despite the large values reported for the complexes, both do not possess SIM behavior under any applied fields. We have explicitly studied the electronic structure of these complexes to have a fundamental understanding of this peculiar behavior. We strive to accomplish this by probing their magnetic relaxation pathways. Complexes **4** and **5** are also experimentally synthesized by Ni et al.[36] and Ung et al.[37] respectively. However, to the best of our knowledge, there is no report on the magnetic characteristics of the complexes. Possessing underlying requisites for superior SIMs i.e., linear structure and Fe(I) metal center and hence, unquenched orbital angular momentum, we speculate if the later complexes could manifest themselves

4

as potential contenders for SIMs. Consequently, we have scrutinized the two complexes to investigate their magnetic anisotropy and hence, their potential to act as SIMs.
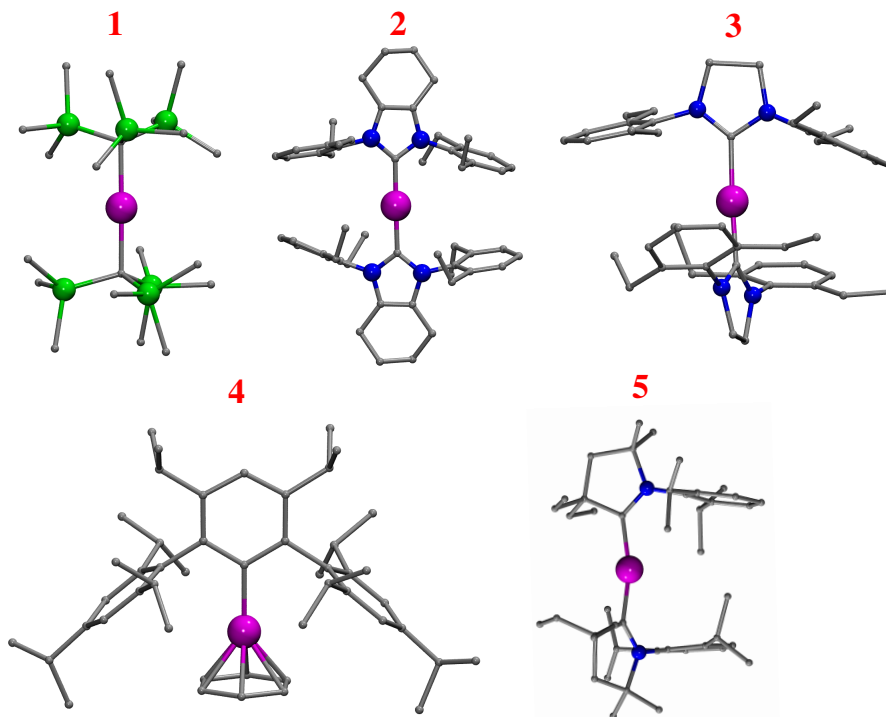

Figure 1: Complexes under study. $[\text{Fe}\{\text{C}(\text{SiMe}_3)\}_3]^{-1}$ **(1)**; $[\text{Fe}(\text{cyIDep})_2]^{+1}$ **(2)**; $[\text{Fe}(\text{sIDep})_2]^{+1}$ **(3)**; $[(\eta^6\text{-}\text{C}_6\text{H}_6)\text{FeAr}^*\text{-}3,5\text{-}\text{Pr}_2^i]$ **(4)**; $[(\text{CAAC})_2\text{Fe}]^{+1}$ **(5)**. SiMe$_3$ = trimethylsilyl; cyIDep = 1,3-bis(2′,6′-diethylphenyl)-4,5-(CH$_2$)$_4$-imidazol-2-ylidene; sIDep = 1,3-bis(2′,6′-diethylphenyl)-imidazolin-2-ylidene; Ar*-3,5-Pr$_2^i$ = C$_6$H-2,6-(C$_6$H$_2$-2,4,6-Pr$_3^i$)$_2$-3,5-Pr$_2^i$; CAAC = cyclic (alkyl)(amino)carbene. Colour code: Pink for Fe, Blue for N, Green for Si, Gray for C. Hydrogens are omitted for clarity.

2 Computational Details

All the ground and excited state energies and wave function calculations are performed on the experimentally reported X-ray crystal structures' geometries. The molecular coordinate system is chosen in such a way that Fe(I) is the origin of the coordinate system and the z-axis points approximately towards the ligands. The correlated calculations are done using Complete Active Space Self Consisent Field (CASSCF)[38] together with N-Electron Valence Perturbation Theory (NEVPT2).[39] The Fe(I) possess d^7 electronic configuration giving rise

to 10 quartets (S=3/2) and 40 doublets (S=1/2) states. To benchmark the methodology, we performed the calculation for complex **1** considering all the roots of quartet and doublet and another calculation with all roots of quartet only. However, the doublet states do not show any significant contribution to the D values, therefore, the calculations are performed accounting for only 10 quartet states (see Table S1 in SI). The CASSCF energy levels are obtained by state-averaging these states in the active space consisting of 7 electrons distributed in 5 3d orbitals i.e., CAS (7,5). The effect of dynamical correlations is included by performing NEVPT2 calculations on top of CASSCF converged wavefunction. Scalar relativistic effects are taken into account employing second-order Douglas-Kroll-Hess triple-DKH-def2-TZVP basis set[40] and auxiliary basis set is generated automatically using AUTOAUX keyword.[41] Tight self-consistent field (SCF) convergence criteria (10^{-10} au) is used in all the calculations. The spin-orbit interactions along with the zeeman interactions are incorporated by the quasi-degenerate perturbation theory (QDPT) approach.[42,43] Magnetic parameters (D, E/D and g-tensors) have been computed using effective Hamiltonian theory as implemented in the ORCA (4.0.1.2) program package.[44,45] Ab initio ligand field theory (AILFT) analysis based on wavefunction obtained from SA-CASSCF/NEVPT2 has been employed to obtain precise d-orbital splitting pattern of the studied complexes.[46] Ab initio blocking barriers for relaxation mechanisms have been computed from SINGLE_ANISO module as implemented in Orca v5.0.1. The *ab initio* CASSCF and CASPT2 calculations are also performed in Open-Molcas (19.11).[47,48] For CASSCF calculations in OpenMolcas, the relativistic contracted atomic natural orbital type basis sets i.e., [ANO-RCC...5s4p2d] for Fe, [ANO-RCC...4s3p] for Si, [ANO-RCC...3s2p] for N and C and [ANO-RCC...2s] for H are employed.[49] To account for spin-orbit effects, AMFI spin-orbit operator is used and DKH Hamiltonian is considered for scalar relativistic effect. The AMFI (atomic mean field integral) spin–orbit operator is introduced to account for the spin–orbit effects. The scalar relativistic effect is considered using the DKH Hamiltonian. The resolution-of-identity approximation is employed to accelerate the calculation.[50]

3 Results and Discussion

3.1 ZFS parameters and *g* tensors

For complex **1**, the alternating current magnetic susceptibility measurements yield high value of spin reversal barrier i.e., $U_{eff} = 226$ cm^{-1}.[29] The large U_{eff} value is the result of unquenched orbital angular momentum, thereby, maximizing the magnetic moment. The computed D value from SA-CASSCF calculations is -102.16 cm^{-1} which further enhances to -109.13 cm^{-1} when dynamical correlations are taken into account employing NEVPT2. Since for non-integral spin complexes, U_{eff} corresponds to $|D|(S^2-1/4)$, the D value of -109.13 cm^{-1} leads to U_{eff} of 218.26 cm^{-1}. The value is in nice agreement with the experimentally observed value of 226 cm^{-1}. Moreover, the D value of -108.55 cm^{-1} is obtained from MS-CASPT2 calculations, in nice agreement with that obtained from NEVPT2 For all the studied complexes, the SA-CASSCF/NEVPT2 and MS-CASPT2 computed D values are collected in Table 1. For complexes **2**, **4** and **5**, negative D value is obtained from NEVPT2 with moderate magnitude in the range -33 to -80 cm^{-1}. However, a positive D value of 40.30 cm^{-1} is observed for complex **3**. CASPT2 also results in negative D values for complexes **2**, **4** and **5** with comparable magnitude as obtained from NEVPT2 calculations. However, a discrepancy is observed between the computed D value for complex **3** for which NEVPT2 yields +45.34 cm^{-1} in contrast to the CASPT2 value of -25.84 cm^{-1}, although +34 cm^{-1} is reported by DDCI3 calculations by Meng et al.[34] The value reported by CASPT2 in contrast to NEVPT2 and DDCI3 may be attributed to the issue of intruder states. Owing to large D value, complex **4** proffers itself as the second Fe(I) centred complex with large ZFS among other linear Fe(I) complexes reported so far with relatively low spin-reversal barrier.

For complexes with negative value of D, the Kramers doublet with the maximum spin projection is the ground-state while reverse is true with positive D value.[51] The negative value of D for all complexes except **3** implies that the Kramers doublets (KDs), with the

projection of total angular momentum $m_J = \pm 7/2$ is the ground state for these complexes. However, for complex **3** with positive D value, the ground state KDs has $m_J = \pm 1/2$ as the projection of total angular momentum.

Table 1: SA-CASSCF/NEVPT2 and MS-CASPT2 computed D values for all the studied Fe(I) complexes.

Complexes	SA-CASSCF[a]		SA-NEVPT2[a]		SA-CASSCF[b]		MS-CASPT2[b]	
	D	$\|E/D\|$	D	$\|E/D\|$	D	$\|E/D\|$	D	$\|E/D\|$
1[c]	-102.16	0.0004	-109.13	0.0004	-106.08	0.0003	-108.55	0.0002
2[d]	-68.89	0.1745	-33.32	0.0475	-78.85	0.1223	-28.32	0.0824
3[d]	42.38	0.0918	40.30	0.2475	45.34	0.1244	-25.84[e]	0.3219
4	-90.23	0.0038	-79.06	0.0046	-90.29	0.0049	-67.97	0.0067
5	-24.77	0.2837	-65.10	0.0467	-27.24	0.2071	-21.96	0.2282

[a]The calculations are performed with DKH-def2-TZVP basis set in Orca.
[b]The calculations are performed with ANO-RCC-VDZ basis set in OpenMolcas.
[c]The spin reversal barrier (U_{eff}) of 226 cm^{-1} is reported experimentally.[30]
[d]The D value of -62.4 cm^{-1} and 34.0 cm^{-1} for **2** and **3** respectively are reported from DDCI3 method by Meng et al.[34]
[e]The contrasting negative sign of D is may be due to the issue of intruder states in CASPT2.

For a molecule to possess uniaxial anisotropy with slow relaxation of magnetization under no applied field, apart from negative axial ZFS (D), the negligibly small rhombicity i.e., $|E/D|$ ratio is required.[52] The non-zero value of E allows mixing of $\pm M_s$ levels, leading to relaxation of electron through quantum tunneling.[53] The SA-CASSCF/NEVPT2 computed $|E/D|$ ratio of all the complexes are collected in Table 1. Complexes **1** and **4** exhibit negligibly small rhombicity i.e., $|E/D|$ <0.005 (Table 1) indicating infinitesimal transition probability of relaxation through quantum tunneling of magnetization (QTM) within the ground-state Kramers doublet. Complexes **2** and **5** possess small $|E/D|$ ~0.04, implying partial relaxation through quantum tunneling of magnetization within the ground-state Kramers doublet. However, for complex **3**, large $|E/D|$ is observed indicating relaxation of magnetization through the ground-state Kramers doublet.

Besides ZFS parameters, the g tensor corresponding to a pair of KDs, which imparts the preferential direction of magnetization in a particular spin-orbit state, is an important

parameter for governing the efficiency of SIMs.[54] Complexes with $g_z > g_y \approx g_x$ are characterized with easy axis anisotropy with g_z as the favorable direction of magnetization. In contrast, $g_y \approx g_x > g_z$ signifies easy plane anisotropy and $g_z > g_y > g_x$ represents the case of triaxial anisotropy.[55]

Table 2: Computed g tensors for the lowest four Kramers doublets for all the complexes

Complexes	Kramers doublet (cm^{-1})		g_x	g_y	g_z	g_z angle (deg)
1	0	$\pm 7/2$	0.0021	0.0021	9.9706	0
	218.27	$\pm 5/2$	0.9850	0.9868	5.8763	0.05
	460.56	$\pm 1/2$	0.9646	1.0073	1.8743	0.41
	710.06	$\pm 3/2$	0.0110	0.0154	2.0360	0.02
2	0	$\pm 7/2$	0.3881	0.4128	10.2543	0
	66.88	$\pm 5/2$	2.7605	3.6506	7.3288	67.51
	124.74	$\pm 1/2$	0.3713	0.8840	7.9411	89.14
	328.16	$\pm 3/2$	0.2771	0.6426	9.1012	83.49
3	0	$\pm 1/2$	1.6345	3.2055	7.5223	0
	87.70	$\pm 3/2$	1.8871	1.9675	5.5227	89.98
	754.08	$\pm 7/2$	0.7034	1.9056	8.6470	89.88
	940.57	$\pm 5/2$	2.3501	3.3439	3.4798	4.07
4	0	$\pm 7/2$	0.0291	0.0299	9.5162	0
	158.13	$\pm 5/2$	3.4048	3.4129	4.2463	0.0
	523.70	$\pm 1/2$	0.2080	3.2439	3.5724	89.99
	701.54	$\pm 3/2$	0.1144	0.1323	2.6439	0.0
5	0	$\pm 7/2$	0.3104	0.3611	9.7200	0
	130.64	$\pm 5/2$	0.4034	0.9040	5.7278	6.17
	293.58	$\pm 1/2$	1.8417	3.0274	4.3019	89.27
	584.26	$\pm 3/2$	1.5647	1.8859	3.6593	89.71

The g tensors for the ground-state and the lowest three excited states of all the complexes are shown in Table 2. For complexes **1** and **4**, the computed g tensors in the ground-state KDs are observed to show $g_z >> g_y \approx g_x$, indicating g_z as the favorable direction of magnetization with strong Ising type nature. This uniaxial magnetic anisotropy signifies negligible relaxation of magnetization from the ground state Kramers pair. However, for

the first and higher excited states, the extent of uniaxiality is reduced. Moreover, along with the changes in g, the direction of magnetization of the excited state from the ground state (measured as g_z angle in Table 2) also deviates. These decreased uniaxiality and non-coincidence of the anisotropy axis of excited state with respect to the ground-state leads to faster relaxation of magnetization from the corresponding state.[54] For complexes **2** and **5**, although the g-tensor show axiality with $g_z >> g_y \approx g_x$, but lacks pure Ising nature. This suggests partial tunneling within the ground state KDs along with faster tunneling through the excited state with reduced uniaxiality and deviation of anisotropy axis from the ground state. Complex **3** is a peculiar case possessing triaxial anisotropy with $g_z > g_y > g_x$. This triaxial anisotropy has been observed earlier also for Co(II) compounds by Møller et al.[55] and Korchagin et al.[56]

3.2 Origin of ZFS

To gain a better understanding of the observed magnitude as well as the sign of D values for the studied complexes, we have analyzed the pattern of molecular d-orbitals splitting of these complexes obtained from AILFT analysis as shown in the top panel of Figure 2. For **1**, the d-orbital splitting is observed where the d_{z^2} is lowest in energy followed by closely degenerate pairs of $d_{x^2-y^2}$ and d_{xy} and then by d_{xz} and d_{yz}. The stabilization of d_{z^2} is a result of strong $3d_{z^2}$-$4s$ mixing as reported by Zadrozny et al.[29] Visual inspection of the shape of d_{z^2} orbital (bottom of Figure 2) reveals an appreciable overlap where the donut-like ring in the xy plane of d_{z^2} orbital mixes with the $4s$ orbital. This $3d_{z^2}$-$4s$ mixing is observed for all the complexes. Moreover, this $3d_{z^2}$-$4s$ is also evident from the analysis of Löwdin orbital composition of the $3d$-orbitals (Table S2). The d_{z^2} orbital is observed to have a composition of $\sim 80\%$ with appreciable s-orbital character ($\sim 10\%$), however, the other d-orbitals are pure with $\sim 95\%$ composition. This pattern of d-orbital ordering of complex **1** results into the ground state with dominant electronic contribution from $d_{z^2}^2 d_{x^2-y^2}^2 d_{xy}^1 d_{xz}^1 d_{yz}^1$ and the first excited state has the major electronic contribution from $d_{z^2}^2 d_{x^2-y^2}^1 d_{xy}^2 d_{xz}^1 d_{yz}^1$. Since the energy gap between the

10

ground and first excited state is very small i.e., 56.0 cm^{-1} (Table 3) and the excitation of an electron from ground to first excited state takes place between the same $|m_l|$ states, thus, the spin-conserved transition from $d_{x^2-y^2}$ to d_{xy} leads to large negative contribution to the D value. The second excited state is composed of several determinants with major contribution from $d_{z^2}^1 d_{x^2-y^2}^2 d_{xy}^2 d_{xz}^1 d_{yz}^1$. Here, the electron promotes to the states with different $|m_l|$ values and the energy difference between the ground and second excited state is quite large (Table 3), hence, it gives a small positive contribution to the D value. Since the first excited state lies close to the ground-state, it governs the overall sign and magnitude of D leading to a high negative D value of -109.13 cm^{-1} for complex **1**.

For complex **2**, d_{z^2} orbital is again stabilized, however, in this complex, d_{xz} and d_{yz} orbitals are more stabilized as compared to d_{xy} and $d_{x^2-y^2}$ orbitals which is in contrast to the d-orbital splitting pattern observed for complex **1**. The significant interactions of the d_{xz} and d_{yz} orbitals of the Fe atom with the π-orbitals of the carbene ligand via $p\pi$-$d\pi$ interactions lead to stabilization of d_{xz} and d_{yz}. A considerable overlap between the carbene $p\pi$ type orbitals and metal d_{xz} and d_{yz} orbitals is visualized in Figure 2. Although the d_{xz} and d_{yz} are lower in energy, the complex possesses *non-Aufbau* ground state with electronic configuration, $d_{z^2}^2 d_{xz}^1 d_{yz}^1 d_{xy}^2 d_{x^2-y2}^1$. The *non-Aufbau* electronic ground-state was also observed by Bunting et al. for Co(II) complex[22] and Ruiz et al. for ferrocenium complex.[57] The viable reason for this anomalous configuration is the small energy difference of d_{z^2} with d_{xz} and d_{yz} i.e., 0.097 and 0.174 eV respectively (Table S4). Since these d-orbitals are quasi-degenerate, therefore, to avoid inter-electronic repulsion for the *Aufbau* configuration i.e., $d_{z^2}^2 d_{xz}^2 d_{yz}^1 d_{xy}^1 d_{x^2-y2}^1$, the complex exhibits *non-Aufbau* ($d_{z^2}^2 d_{xz}^1 d_{yz}^1 d_{xy}^2 d_{x^2-y2}^1$) electronic arrangement. Further, the first excited state will be attained by promoting an electron from d_{xy} to $d_{x^2-y^2}$ with small energy difference (52.0 cm^{-1}) and between same $|m_l|$ states leading to large negative contribution to the D value. The second excited state has the major contribution from $d_{z^2}^2 d_{xz}^1 d_{yz}^2 d_{xy}^1 d_{x^2-y2}^1$ attained by transfer of an electron from d_{xy} to d_{yz} with small energy difference (143.7 cm^{-1}), leading to significant positive contribution to the D value. Thus, although the overall D

11

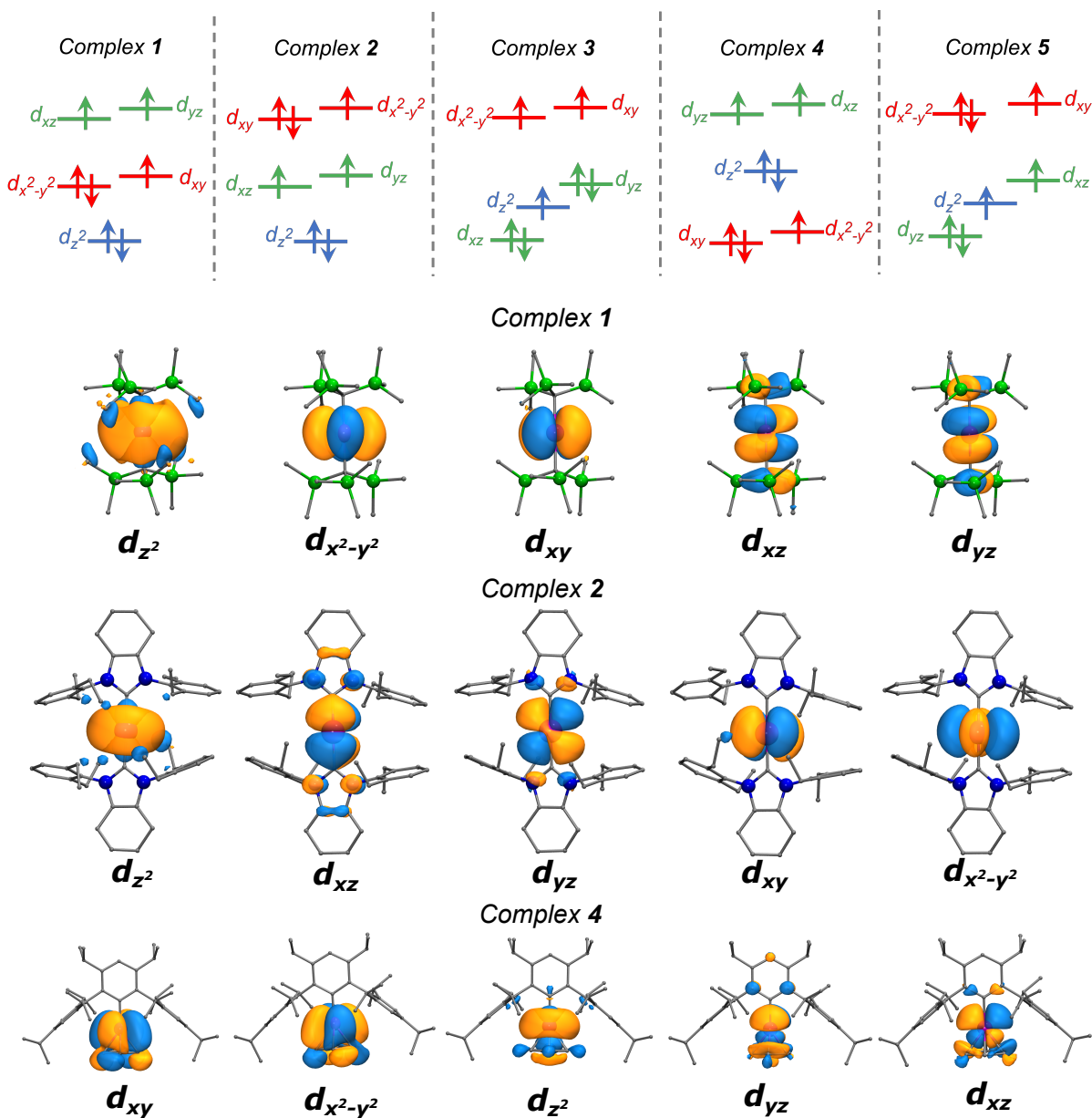value is negative but the magnitude is smaller due to large positive contribution from the second excited state.

Figure 2: The pattern of *d*-orbital splitting of all the complexes and the molecular *d*-orbitals obtained from SA-CASSCF/NEVPT2 calculations with active space of CAS(7,5) for complexes **1**, **3** and **4**.

In complex **3**, the imidazolin ylidine ligand is substituted which, due to better π accepting ability than imidazol ylidine[58] (in complex **2**), renders more pronounced $d\pi$-$p\pi$ interactions

and hence, stabilizes the d_{xz} orbital compared with the d_{z^2} and d_{yz} which are almost degenerate (Figure S1). As a consequence of this pattern of d-orbital splitting, the ground state acquires *non-Aufbau* electronic configuration, $d_{xz}^2 d_{z^2}^1 d_{yz}^2 d_{x^2-y^2}^1 d_{xy}^1$ (similar to **2**). Since, the first and second excited states are achieved by promoting an electron from d_{yz} to $d_{x^2-y^2}$ and d_{xy} respectively with different $|m_l|$ states, both of them give a positive contribution to the D value. Hence, the complex exhibits an overall positive D value. Thus, the different splitting pattern due to better π-acceptor imidazoline ylidine than imidazol ylidine (in **2**) results in opposite signs of magnetic anisotropy for the two complexes. Another difference between the two molecules is the dihedral angle between the ligands attached to the complexes. Complex **2** renders dihedral angle of 14° in contrast to the large dihedral angle of 70° exhibited by complex **3** (tabulated in Table S10). The different dihedral angles can also be the underlying rationale for the contrasting signs of magnetic anisotropy for the complexes **2** and **3** as also observed in Co complexes by Meng et al.[58]

The complex **4** is a peculiar case where quasi-degenerate d_{xy} and $d_{x^2-y^2}$ are lower in energy as compared to d_{z^2}. The analysis of molecular orbitals as shown in Figure 2 reveals a substantial overlap between the d_{xy} and $d_{x^2-y^2}$ orbitals of Fe with the π-electron cloud of the benzene ring which is binding to the Fe through η^6 fashion making a half-sandwich complex. The π-electron cloud of the benzene ring and the d_{xy} and $d_{x^2-y^2}$ orbitals of the Fe atom are lying perpendicular to the molecular axis. These orbitals can be considered as a linear combination of $p\pi$ orbitals of the benzene ring and d-orbitals (d_{xy} and $d_{x^2-y^2}$) of Fe atom indicating significant interactions and hence leading to substantial stabilization of these orbitals followed by d_{z^2} and subsequently by a closely degenerate pair of d_{xz} and d_{yz} orbitals. The outcome of this d-orbital ordering is the ground-state with electronic configuration $d_{xy}^2 d_{x^2-y^2}^1 d_{z^2}^2 d_{yz}^1 d_{xz}^1$. The promotion of electron from d_{xy} to $d_{x^2-y^2}$ i.e., between same $|m_l|$ states and with small energy difference (298.3 cm^{-1}) leads to first excitation providing large negative contribution to D value. Further, the second excited state is obtained by transfer of electron from d_{z^2} to $d_{x^2-y^2}$ causing small positive contribution to the D value, with overall

13

negative magnetic anisotropy for the complex.

Complex **5**, accomodating CAAC ligand, a good π-accepting ligand, possesses d-orbital splitting pattern similar to that obtained for complex **3** with the only difference showing interchange of d_{yz} and d_{xz} orbitals. However, unlike complex **3**, the ground state electronic configuration for this complex is different with dominant contribution from $d_{yz}^2 d_{z^2}^1 d_{xz}^1 d_{x^2-y^2}^2 d_{xy}^1$ and the first excited state is obtained by transfer of electron from $d_{x^2-y^2}$ to d_{xy} with significant negative contribution to D value due to smaller energy gap (54.0 cm^{-1}). The second excited state is attained by electron transfer from d_{yz} to d_{z^2} giving notable positive contribution to D value. And the complex exhibits overall negative D value.

Thus, the different D values exhibited by these complexes are a result of distinct d-orbital splitting patterns caused by different ligands attached to the metal center, Fe(I).

Table 3: Lowest spin-free energy levels of the complexes with their individual contribution to D computed using SA-CASSCF/NEVPT2 with (7,5) active space.

Complex	Excited states	Spin-free states (cm^{-1})	Contb. D (cm^{-1})
1	1	56.0	-119.02
	2	5380.2	02.94
2	1	52.0	-103.54
	2	143.7	31.26
3	1	791.5	24.41
	2	1459.3	09.85
4	1	298.3	-85.19
	2	924.7	01.43
5	1	54.0	-112.24
	2	774.0	22.23

3.3 Mechanism of magnetic relaxation

To have a qualitative understanding of the mechanism of magnetic relaxation, we have plotted *ab-initio* blocking barriers computed from SINGLE_ANISO approach as implemented in Orca as shown in Figure 3. The relaxation of magnetization can occur through three probable mechanistic pathways namely a) quantum tunneling of magnetization (QTM) within the

ground KDs b) Orbach/Raman relaxation process where Raman relaxation process takes place through virtual transitions c) thermally assisted quantum tunneling of magnetization (TA-QTM) within excited KDs.[15] In the computed relaxation mechanism, the KDs are presented according to their magnetic moments. The numbers at each arrow connecting any two energy levels represent the matrix elements of transition-magnetic-moments between the connecting energy levels.

For complex **1** and **4**, the transition-magnetic-moment matrix elements between the ground state KDs are negligibly small i.e., 0.0007 and 0.009 respectively, ruling out the possibility of QTM through the ground state in these complexes. In addition to this, the calculated transition-magnetic-moment matrix element between the ground and first excited KDs of opposite magnetic moments are also very small in magnitude (0.0008 and 0.01 for **1** and **4** respectively), implying slow Orbach relaxation. However, the large transversal-magnetic-moment (0.32 for **1** and 1.1 for **4**) for the first excited state suggests relaxation to be operative through first excited state via TA-QTM.

In the case of complexes **2** and **5**, the computed transveral-magnetic-moment is 0.14 and 0.1 respectively in the ground state suggesting partial QTM to be operative through the ground state KDs. The larger magnitude of transition-magnetic-moment matrix elements of 1.3 and 1.1 for **2** and **5** respectively for the first excited state for both the complexes mark the major relaxation to proceed through this state. Besides, the off-diagonal matrix elements between the ground and first excited KDs of opposite magnetization are also moderate (0.42 and 1.0) opening up further relaxation pathways via Orbach relaxation. Therefore, for these complexes, multiple relaxation pathways are operational. On the other hand, for complex **3**, the $m_J = \pm 1/2$ is the ground state with a barrierless potential well which is also signified by the high magnitude of transition-magnetic-moment matrix element i.e., 1.8, suggesting faster relaxation within the ground state for this complex.
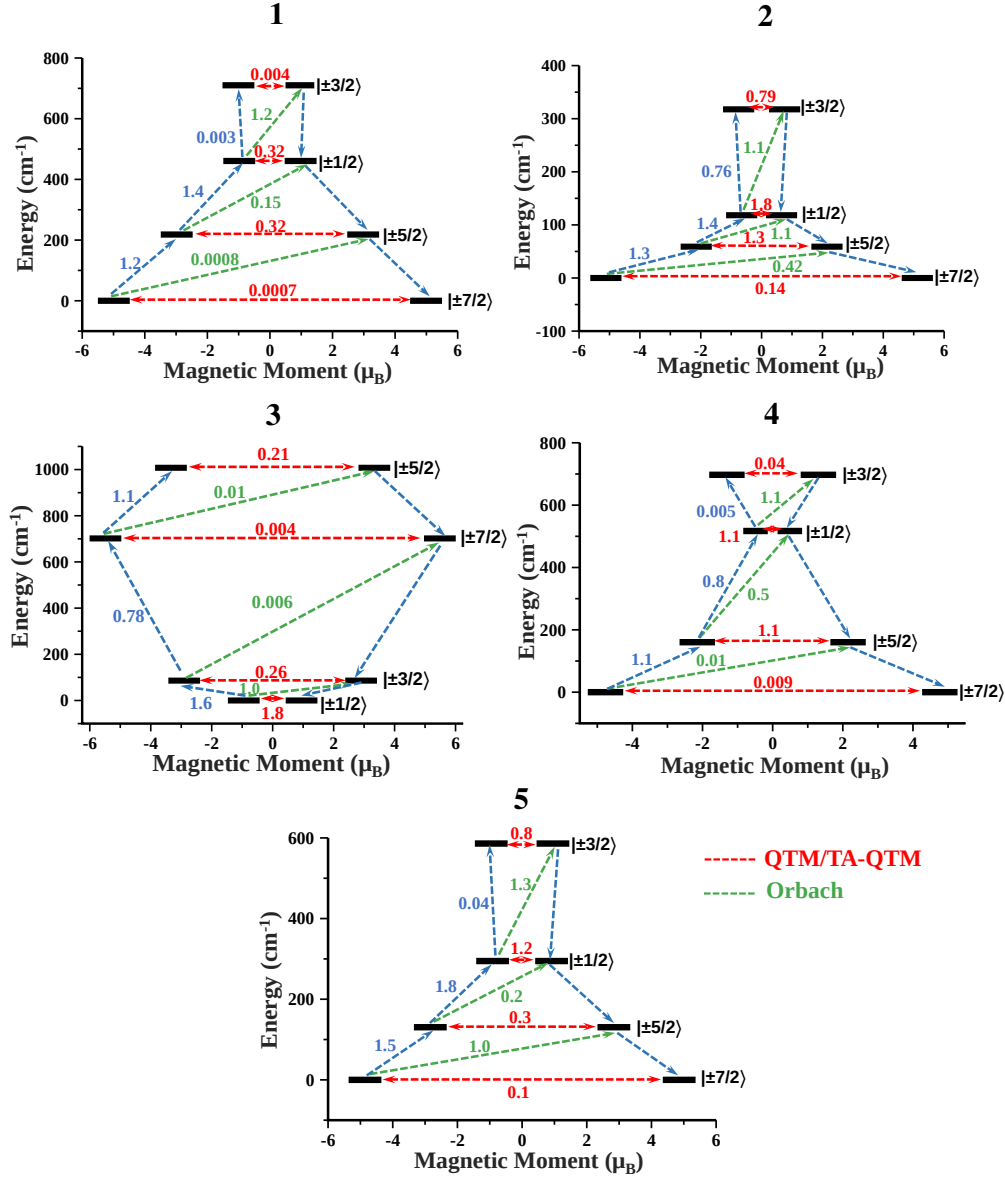
Figure 3: Ab initio magnetization blocking barrier for all the complexes. The black lines represent the Kramers doublets (KDs) as a function of the magnetic moment. The dotted red lines represent the QTM/TA-QTM. The dotted green lines denote the Orbach relaxation pathways. The dotted blue lines show the most probable relaxation pathway. The numbers at each connecting arrow represent transition-magnetic-moment matrix elements.

These relaxation pathways provide the plausible reason for no SIM behaviors under any applied field for complexes **2** and **3** as observed by Meng et al.[34] Since for complex **2**, due to multiple relaxation pathways i.e., partial QTM through the ground-state KDs and Orbach relaxation, the complex shows absence of SIM behavior. In contrast, complex **3** possessing

barrierless potential well leads to relaxation within the ground-state KDs. Thus, both the complexes do not show any signatures of SIM behavior.

4   Conclusion

We have investigated the origin of single molecule magnetic behavior of a series of linear or quasi-linear Fe(I) complexes employing state-of-the-art *ab initio* calculations. The different *d*-orbital splitting patterns are manifested by the complexes which is the ramification of the intrinsic nature of the ligands attached to the complex. Since the energetic ordering of *d*-orbitals is the decisive parameter for the magnitude and sign of zero field splitting parameter, all complexes except **1**, possess the *non-Aufbau* electronic ground state due to small energy difference in the *d*-orbitals showing a range of D values from -33 to -109 cm^{-1} and even positive D value for one of the complex. Complexes **2** and **3** are reported with absence of SIM behavior under any field, however, opposite signs of D value (negative for **2** and positive for **1**) are shown from *ab initio* calculations.[34] This observation is rationalized based on different patterns of *d*-orbital splitting and their ground state occupancy. Moreover, the existence of multiple relaxation pathways with partial relaxation within ground state KDs for complex **2** and barrierless potential well triggering faster relaxation within the ground state KDs in complex **3** provides signatures for the absence of SIM behavior in these complexes. Thus, moderate magnitude of magnetic anisotropy and faster quantum tunneling of relaxation are found to co-exist in these complexes. Moreover, the experimentally synthesized complexes **4** and **5** are characterized with large magnetic anisotropy of -79.06 and -65.10 cm^{-1} but complex **5** exhibits multiple relaxation pathways with partial tunneling within the ground state KDs. Therefore, it is speculated to possess SIM behavior under applied field. However, complex **4** possessing Ising type anisotropy and TA-QTM provide the potential to behave as superior SIM under zero applied field. Moreover, complex **4** is the second Fe(I) complex to possess large ZFS value of -79.06 cm^{-1} followed by complex **1** (D=-109.13 cm^{-1}) among

all other Fe(I) linear complexes reported so far.

Acknowledgement

References

(1) Affronte, M.; Troiani, F.; Ghirri, A.; Candini, A.; Evangelisti, M.; Corradini, V.; Carretta, S.; Santini, P.; Amoretti, G.; Tuna, F., et al. Single molecule magnets for quantum computation. *J. Phys. D: Appl. Phys.* **2007**, *40*.

(2) Gaita-Ariño, A.; Luis, F.; Hill, S.; Coronado, E. Molecular spins for quantum computation. *Nat. Chem.* **2019**, *11*, 301–309.

(3) Hymas, K.; Soncini, A. Molecular spintronics using single-molecule magnets under irradiation. *Phys. Rev. B* **2019**, *99*, 245404.

(4) Cavallini, M.; Gomez-Segura, J.; Ruiz-Molina, D.; Massi, M.; Albonetti, C.; Rovira, C.; Veciana, J.; Biscarini, F. Magnetic information storage on polymers by using patterned single-molecule magnets. *Angew. Chem. Int. Ed.* **2005**, *44*, 888–892.

(5) Gatteschi, D.; Sessoli, R.; Villain, J. *Molecular nanomagnets*; Oxford University Press on Demand, 2006; Vol. 5.

(6) Ishikawa, N.; Sugita, M.; Ishikawa, T.; Koshihara, S.-y.; Kaizu, Y. Lanthanide double-decker complexes functioning as magnets at the single-molecular level. *J. Am. Chem. Soc.* **2003**, *125*, 8694–8695.

(7) Tang, J.; Zhang, P. *Lanthanide single molecule magnets*; Springer, 2015.

(8) Woodruff, D. N.; Winpenny, R. E.; Layfield, R. A. Lanthanide single-molecule magnets. *Chem. Rev.* **2013**, *113*, 5110–5148.

(9) Marin, R.; Brunet, G.; Murugesu, M. Shining new light on multifunctional lanthanide single-molecule magnets. *Angew. Chem. Int. Ed.* **2021**, *60*, 1728–1746.

(10) Guo, F.-S.; Day, B. M.; Chen, Y.-C.; Tong, M.-L.; Mansikkamäki, A.; Layfield, R. A. Magnetic hysteresis up to 80 kelvin in a dysprosium metallocene single-molecule magnet. *Science* **2018**, *362*, 1400–1403.

(11) Goodwin, C. A.; Ortu, F.; Reta, D.; Chilton, N. F.; Mills, D. P. Molecular magnetic hysteresis at 60 kelvin in dysprosocenium. *Nature* **2017**, *548*, 439–442.

(12) McClain, K. R.; Gould, C. A.; Chakarawet, K.; Teat, S. J.; Groshens, T. J.; Long, J. R.; Harvey, B. G. High-temperature magnetic blocking and magneto-structural correlations in a series of dysprosium (III) metallocenium single-molecule magnets. *Chem. Sci.* **2018**, *9*, 8492–8503.

(13) Craig, G. A.; Murrie, M. 3d single-ion magnets. *Chem. Soc. Rev.* **2015**, *44*, 2135–2147.

(14) Perlepe, P. S.; Maniaki, D.; Pilichos, E.; Katsoulakou, E.; Perlepes, S. P. Smart ligands for efficient 3d-, 4d-and 5d-metal single-molecule magnets and single-ion magnets. *Inorganics* **2020**, *8*, 39.

(15) Frost, J. M.; Harriman, K. L.; Murugesu, M. The rise of 3-d single-ion magnets in molecular magnetism: towards materials from molecules? *Chem. Sci.* **2016**, *7*, 2470–2491.

(16) Reiff, W. M.; LaPointe, A. M.; Witten, E. H. Virtual free ion magnetism and the absence of Jahn- Teller distortion in a linear two-coordinate complex of high-spin iron (II). *J. Am. Chem. Soc.* **2004**, *126*, 10206–10207.

(17) Power, P. P. Stable two-coordinate, open-shell (d^1–d^9) transition metal complexes. *Chem. Rev.* **2012**, *112*, 3482–3507.

(18) Mossin, S.; Tran, B. L.; Adhikari, D.; Pink, M.; Heinemann, F. W.; Sutter, J.; Szilagyi, R. K.; Meyer, K.; Mindiola, D. J. A mononuclear Fe (III) single molecule magnet with a 3/2 - 5/2 spin crossover. *J. Am. Chem. Soc.* **2012**, *134*, 13651–13661.

(19) Yao, B.; Singh, M. K.; Deng, Y.-F.; Wang, Y.-N.; Dunbar, K. R.; Zhang, Y.-Z. Trigonal prismatic cobalt (II) single-ion magnets: Manipulating the magnetic relaxation through symmetry control. *Inorg. Chem.* **2020**, *59*, 8505–8513.

(20) Feng, X.; Hwang, S. J.; Liu, J.-L.; Chen, Y.-C.; Tong, M.-L.; Nocera, D. G. Slow magnetic relaxation in intermediate spin S= 3/2 mononuclear Fe(III) complexes. *J. Am. Chem. Soc.* **2017**, *139*, 16474–16477.

(21) Khurana, R.; Gupta, S.; Ali, M. E. First-principles investigations of magnetic anisotropy and spin-crossover behavior of Fe (III)–TBP complexes. *J. Phys. Chem. A* **2021**, *125*, 2197–2207.

(22) Bunting, P. C.; Atanasov, M.; Damgaard-Møller, E.; Perfetti, M.; Crassee, I.; Orlita, M.; Overgaard, J.; van Slageren, J.; Neese, F.; Long, J. R. A linear cobalt (II) complex with maximal orbital angular momentum from a non-Aufbau ground state. *Science* **2018**, *362*.

(23) Chowdhury, S. R.; Mishra, S. Large magnetic anisotropy in linear Co^{II} complexes - Ab initio investigation of the roles of ligand field, structural distortion, and conformational dynamics. *Eur. J. Inorg. Chem.* **2017**, *659*, 668.

(24) Yao, X.-N.; Du, J.-Z.; Zhang, Y.-Q.; Leng, X.-B.; Yang, M.-W.; Jiang, S.-D.; Wang, Z.-X.; Ouyang, Z.-W.; Deng, L.; Wang, B.-W., et al. Two-coordinate Co(II) imido complexes as outstanding single-molecule magnets. *J. Am. Chem. Soc.* **2017**, *139*, 373–380.

(25) Nain, S.; Khurana, R.; Ali, M. E. Harnessing colossal magnetic anisotropy in sandwiched $3d^2$-metallocenes. *ChemRxiv* **2021**, DOI:10.33774/chemrxiv-2021-dbwcv.

(26) Sarkar, A.; Dey, S.; Rajaraman, G. Role of coordination number and geometry in controlling the magnetic anisotropy in Fe(II), Co(II), and Ni(II) single-ion magnets. *Chem. Eur. J.* **2020**, *26*, 14036–14058.

(27) Zadrozny, J. M.; Atanasov, M.; Bryan, A. M.; Lin, C.-Y.; Rekken, B. D.; Power, P. P.; Neese, F.; Long, J. R. Slow magnetization dynamics in a series of two-coordinate iron (II) complexes. *Chem. Sci.* **2013**, *4*, 125–138.

(28) Atanasov, M.; Zadrozny, J. M.; Long, J. R.; Neese, F. A theoretical analysis of chemical bonding, vibronic coupling, and magnetic anisotropy in linear iron (II) complexes with single-molecule magnet behavior. *Chem. Sci.* **2013**, *4*, 139–156.

(29) Zadrozny, J. M.; Xiao, D. J.; Atanasov, M.; Long, G. J.; Grandjean, F.; Neese, F.; Long, J. R. Magnetic blocking in a linear iron (I) complex. *Nat. Chem.* **2013**, *5*, 577–581.

(30) Zadrozny, J. M.; Xiao, D. J.; Long, J. R.; Atanasov, M.; Neese, F.; Grandjean, F.; Long, G. J. Mossbauer spectroscopy as a probe of magnetization dynamics in the linear iron (I) and iron (II) complexes $[Fe(C(SiMe_3)_3)_2]^{1-/0}$. *Inorg. Chem.* **2013**, *52*, 13123–13131.

(31) Werncke, C. G.; Bunting, P. C.; Duhayon, C.; Long, J. R.; Bontemps, S.; Sabo-Etienne, S. Two-coordinate iron (I) complex $[Fe\{N(SiMe_3)_2\}_2]^-$: Synthesis, properties, and redox activity. *Angew. Chem.* **2015**, *127*, 247–250.

(32) Lin, C.-Y.; Fettinger, J. C.; Grandjean, F.; Long, G. J.; Power, P. P. Synthesis, structure, and magnetic and electrochemical properties of quasi-linear and linear iron (I), cobalt (I), and nickel (I) amido complexes. *Inorg. Chem.* **2014**, *53*, 9400–9406.

(33) Ouyang, Z.; Du, J.; Wang, L.; Kneebone, J. L.; Neidig, M. L.; Deng, L. Linear and T-shaped iron (I) complexes supported by N-heterocyclic carbene ligands: Synthesis and structure characterization. *Inorg. Chem.* **2015**, *54*, 8808–8816.

(34) Meng, Y.-S.; Ouyang, Z.; Yang, M.-W.; Zhang, Y.-Q.; Deng, L.; Wang, B.-W.; Gao, S. Multiple magnetic relaxation pathways in T-shaped N-heterocyclic carbene-supported Fe(I) single-ion magnets. *Inorg. Chem. Front.* **2019**, *6*, 1050–1057.

(35) Chakraborty, U.; Demeshko, S.; Meyer, F.; Rebreyend, C.; de Bruin, B.; Atanasov, M.; Neese, F.; Mühldorf, B.; Wolf, R. Electronic structure and magnetic anisotropy of an unsaturated cyclopentadienyl iron (I) complex with 15 valence electrons. *Angew. Chem. Int. Ed.* **2017**, *56*, 7995–7999.

(36) Ni, C.; Ellis, B. D.; Fettinger, J. C.; Long, G. J.; Power, P. P. Univalent transition metal complexes of arenes stabilized by a bulky terphenyl ligand: differences in the stability of Cr(I), Mn(I) or Fe(I) complexes. *Chem. Commun.* **2008**, 1014–1016.

(37) Ung, G.; Rittle, J.; Soleilhavoup, M.; Bertrand, G.; Peters, J. C. Two-coordinate Fe^0 and Co^0 complexes supported by cyclic(alkyl)(amino) carbenes. *Angew. Chem. Int. Ed.* **2014**, *53*, 8427–8431.

(38) Malmqvist, P.-Å.; Roos, B. O. The CASSCF state interaction method. *Chem. Phys. Lett.* **1989**, *155*, 189–194.

(39) Angeli, C.; Cimiraglia, R.; Evangelisti, S.; Leininger, T.; Malrieu, J.-P. Introduction of n-electron valence states for multireference perturbation theory. *J. Chem. Phys.* **2001**, *114*, 10252–10264.

(40) Pantazis, D. A.; Chen, X.-Y.; Landis, C. R.; Neese, F. All-electron scalar relativistic basis sets for third-row transition metal atoms. *J. Chem. Theory Comput.* **2008**, *4*, 908–919.

(41) Stoychev, G. L.; Auer, A. A.; Neese, F. Automatic generation of auxiliary basis sets. *J. Chem. Theory Comput.* **2017**, *13*, 554–562.

(42) Heß, B. A.; Marian, C. M.; Wahlgren, U.; Gropen, O. A mean-field spin-orbit method applicable to correlated wavefunctions. *Chem. Phys. Lett.* **1996**, *251*, 365–371.

(43) Neese, F. Efficient and accurate approximations to the molecular spin-orbit coupling operator and their use in molecular g-tensor calculations. *J. Chem. Phys.* **2005**, *122*, 034107.

(44) Maurice, R.; Bastardis, R.; Graaf, C. d.; Suaud, N.; Mallah, T.; Guihery, N. Universal theoretical approach to extract anisotropic spin hamiltonians. *J. Chem. Theory Comput.* **2009**, *5*, 2977–2984.

(45) Neese, F. The ORCA program system. *Wiley Interdiscip. Rev. Comput. Mol. Sci.* **2012**, *2*, 73–78.

(46) Atanasov, M.; Ganyushin, D.; Sivalingam, K.; Neese, F. In *Molecular Electronic Structures of Transition Metal Complexes II*; Mingos, D. M. P., Day, P., Dahl, J. P., Eds.; Springer Berlin Heidelberg: Berlin, Heidelberg, 2012; pp 149–220.

(47) Fdez. Galvan, I.; Vacher, M.; Alavi, A.; Angeli, C.; Aquilante, F.; Autschbach, J.; Bao, J. J.; Bokarev, S. I.; Bogdanov, N. A.; Carlson, R. K., et al. OpenMolcas: From source code to insight. *J. Chem. Theory Comput.* **2019**, *15*, 5925–5964.

(48) Aquilante, F.; Autschbach, J.; Baiardi, A.; Battaglia, S.; Borin, V. A.; Chibotaru, L. F.; Conti, I.; De Vico, L.; Delcey, M.; Fdez. Galván, I., et al. Modern quantum chemistry with [Open]Molcas. *J. Chem. Phys.* **2020**, *152*, 214117.

(49) Roos, B. O.; Lindh, R.; Malmqvist, P.-Å.; Veryazov, V.; Widmark, P.-O. New Relativistic ANO Basis Sets for Transition Metal Atoms. *J. Phys. Chem. A* **2005**, *109*, 6575–6579.

(50) Aquilante, F.; Pedersen, T. B.; Veryazov, V.; Lindh, R. MOLCAS—a software for multiconfigurational quantum chemistry calculations. *Wiley Interdiscip. Rev. Comput. Mol. Sci.* **2013**, *3*, 143–149.

(51) Boča, R. Zero-field splitting in metal complexes. *Coord. Chem. Rev.* **2004**, *248*, 757–815.

(52) Gatteschi, D.; Sessoli, R. Quantum tunneling of magnetization and related phenomena in molecular materials. *Angew. Chem. Int. Ed.* **2003**, *42*, 268–297.

(53) Freedman, D. E.; Harman, W. H.; Harris, T. D.; Long, G. J.; Chang, C. J.; Long, J. R. Slow magnetic relaxation in a high-spin iron (II) complex. *J. Am. Chem. Soc.* **2010**, *132*, 1224–1225.

(54) Ungur, L.; Chibotaru, L. F. Magnetic anisotropy in the excited states of low symmetry lanthanide complexes. *Phys. Chem. Chem. Phys.* **2011**, *13*, 20086–20090.

(55) Damgaard-Møller, E.; Krause, L.; Lassen, H.; Malaspina, L. A.; Grabowsky, S.; Bamberger, H.; McGuire, J.; Miras, H. N.; Sproules, S.; Overgaard, J. Investigating complex magnetic anisotropy in a Co(II) molecular compound: A charge density and correlated ab initio electronic structure study. *Inorg. Chem.* **2020**, *59*, 13190–13200.

(56) Korchagin, D. V.; Palii, A. V.; Yureva, E. A.; Akimov, A. V.; Misochko, E. Y.; Shilov, G. V.; Talantsev, A. D.; Morgunov, R. B.; Shakin, A. A.; Aldoshin, S. M.; Tsukerblat, B. S. Evidence of field induced slow magnetic relaxation in cis-$[Co(hfac)_2(H2O)_2]$ exhibiting tri-axial anisotropy with a negative axial component. *Dalton Trans.* **2017**, *46*, 7540–7548.

(57) Amoza, M.; Maxwell, L.; Aliaga-Alcalde, N.; Gómez-Coca, S.; Ruiz, E. Spin-phonon coupling and slow-magnetic relaxation in pristine ferrocenium. *Chem. Eur. J.* **2021**, *27*, 16440–16447.

(58) Meng, Y.-S.; Mo, Z.; Wang, B.-W.; Zhang, Y.-Q.; Deng, L.; Gao, S. Observation of the single-ion magnet behavior of d^8 ions on two-coordinate Co(I)–NHC complexes. *Chem. Sci.* **2015**, *6*, 7156–7162.